Supplementary Information

Large-area SHG-CD probes intrinsic chirality in polycrystalline films

Florian Ristow, Kevin Liang, Johannes Pittrich, Jakob Scheffel, Natalie Fehn, Reinhard Kienberger, Ulrich Heiz, Aras Kartouzian*, Hristo Iglev*

Circular dichroism • nonlinear optics • chirality • Second Harmonic Generation

Table of contents

Polarization quality measurements

To verify the polarization quality of the beam, an analyzing polarizer was inserted into the experimental setup between the Pockels cell and the sample, and the beam power was measured behind the analyzer. It was then rotated from 0° to 360° in steps of 15° and the respective powers were measured for each angle. A fit using the Jones calculus was plotted. The elliptical polarized light can be described as a Jones vector, as shown in the following:

$$\vec{E} = \begin{pmatrix} E_x \\ E_y \end{pmatrix} = \begin{pmatrix} a \\ \sqrt{1-a^2}e^{i\varphi} \end{pmatrix} \tag{S1}$$

where $\vec{E}$ is the electric field vector of the incident beam; E_x is the x component and E_y is the y component of the electric field for light propagating in the z-axis. To obtain the intensity, and thus the power (for a known area), the Jones vector in a general elliptical polarization is multiplied by the Jones matrix representing a linear polarizer. Afterwards, the product is multiplied with its complex transpose in order to give the following normalized equation:

$$P(\alpha) = a^2 cos^2\alpha + (1-a^2)sin^2\alpha + a\sqrt{1-a^2}sin2\alpha\, cos\varphi \tag{S2}$$

where a describes the contribution of the two orthogonal linear polarizations of the beam (varies from $0 \leq a \leq 1$); α is the angle induced by the polarizer; and φ is the phase relationship between the two orthogonal linear polarizations. The results can be seen in Figure S1 with the fit parameters $a = 0.708 \pm 0.022\%$ and $\varphi = 1.574 \pm 0.016\%$. For circularly polarized light, one would expect the transmitted power to be independent of the polarizer angle. This behavior is shown in the substantially constant behavior for RCP light. This generally shows good circularity of the beam with a standard deviation of <0.3%.
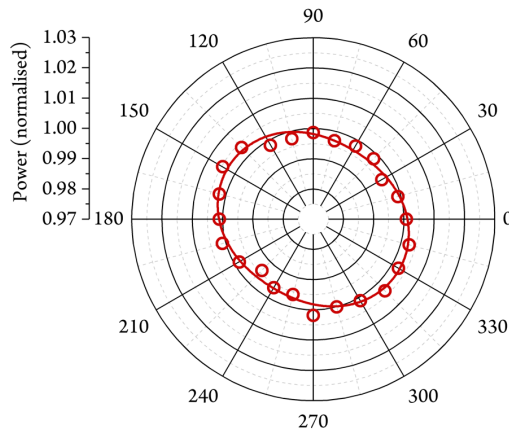

Figure S1: The normalized power of the fundamental incident beam in RCP polarization was recorded at angles from 0° to 360, in steps of 15°. A fit using the Jones calculus was plotted.

Sample preparation procedure

Previous works have already discussed the sample preparation.[1-2] Thin films of enantiopure R-/S-BINOL and racemic BINOL are prepared and evaluated. SHG transmissive fused-silica quartz substrates (Alfa Aeser) with a thickness between 150 and 250 μm are cleaned with spectroscopic acetone and wiped with lens cleaning tissues (ThorLabs). Then, the substrate and the BINOL of our choice is inserted into a vacuum chamber ($<1 \cdot 10^{-6}$ mbar), in which the BINOL is evaporated and adsorbed on to the substrate under high vacuum at room temperature. The evaporation is performed in quartz crucibles with a custom-made molecular beam evaporator. Once a thin film is produced, the vacuum chamber is brought back to atmospheric pressure, from which the thin film is removed and transferred to the laser setup for measurements. All chemicals mentioned are of 99% reagent grade and are purchased from SIGMA-Aldrich. The thickness of the thin film is monitored with a quartz crystal microbalance (QCM; SL-A1E40 from INFICON) and with the use of the Sauerbrey equation,[3] while assuming that all BINOL molecules occupy equal volumes of 357.8 $Å^2$ for an optically active crystal.[4] 20 minutes after the evaporation has finished, the sample was exvacuated and stored and room temperature.

SHG-intensity for varying fundamental beam sizes and power

In Figure S2a, the total absolute SHG intensity (number of counts) of RCP light (orange) and LCP light (green) is plotted against the area of the beam area (mm^2) for pure R-BINOL of 500 nm thickness. The RCP and LCP intensity for each area point is inserted into Equation 1 from the main manuscript in order to obtain the brown line for the R-BINOL in Figure 3a from the main manuscript. Due to in-plane anisotropy, the ratio between RCP and LCP significantly changes with the beam area size for small beam areas. Normally for a constant $\chi^{(2)}$, the two intensity
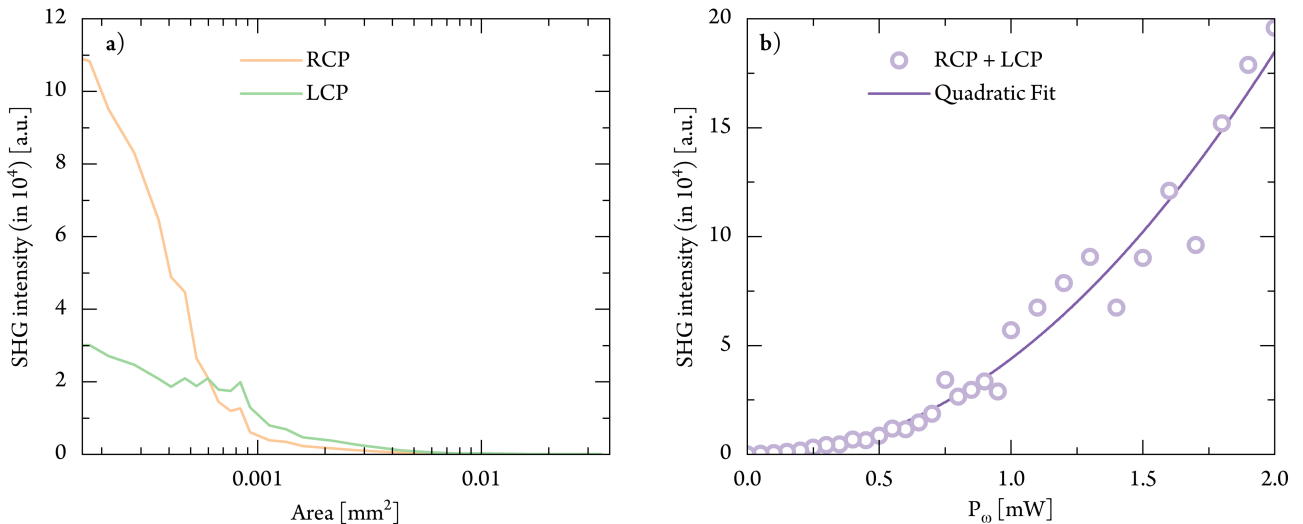

Figure S2: (a) Absolute SHG intensity of RCP (orange) and LCP (green) against the sample area in mm^2 for R-BINOL. For small beam areas, the ratio between of I_{LCP} and I_{RCP} is completely different (even inverted) when compared to the large area case and the curves even intersect. For larger areas, the anisotropic effects average out so the difference between the two polarizations changes. (b) average SHG-intensity changes quadratically with the fundamental power.

curves should just scale by a constant factor and their difference should also scale similarly. The fact that they intersect suggests that there is a change in $\chi^{(2)}$ as the beam area grows more out-of-focus. The intersection is a rough indicator of this change in regime from anisotropic to quasi-isotropic with increasing beam area, as discussed in the "SHG anisotropy for various beam areas" section from the main manuscript. Fig. S2b shows the quadratic dependence of the SHG-intensity when the fundamental intensity is varied. Throughout this measurement, the illuminated sample region remained unchanged, only varying the average power of the fundamental power of the input beam. We refer to our recent study for more information.[1]

Development of in-plane anisotropy over time

Figure S3 shows reflective light microscopy images of enantiopure BINOL for different degrees of crystallization in the film. Herein, the crystallization state in the sample was measured with different sample ages: 30 minutes, 1 day and 9 days after evaporation. The figure illustrates the development of crystallite domains as a function of the sample age. Shortly after evaporation, there is no crystallization in the sample (S3a). The crystal domains emanate from the nucleation center, increasing the in-plane anisotropy in the sample over time (S3b). The morphological activity concludes after 9 days (S3c). All measurement data presented in this manuscript was recorded on fully crystallized samples.
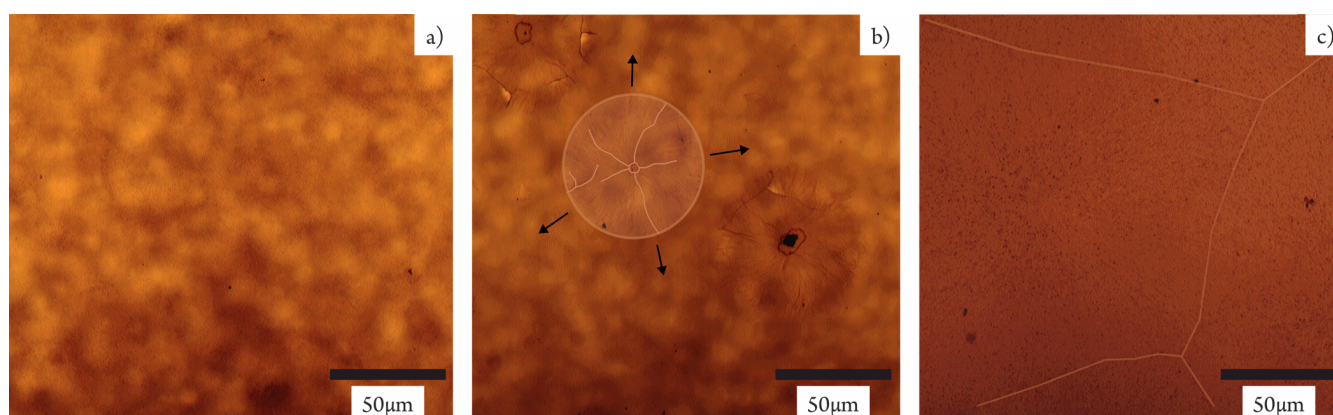

Figure S3: Reflection light microscopy images of enantiopure BINOL (a) 30 minutes after evaporation. No crystallization is visible. (b) 1 day after evaporation: crystallization has started. The outlines of one of the domains is colored and the radial growth direction is indicated with arrows. The sample is partially covered with crystallite domains. (c) 9 days after evaporation. The sample is fully covered with crystallite domains. The outlines of the full domains are colored.

Sample region scanning with different beam sizes

We support the argument of experimental averaging with histogram data (Fig. S4) recorded on crystallized R-BINOL with different beam sizes in the exact same sample region (180x180μm). Experimentally, this was achieved by scanning a small pinhole placed on the film, so that the same sample region was mapped out on a 12x12 grid for a beam diameter of 15μm (6x6 and 3x3 respectively) for front and back illumination. Note that the whole sample region is smaller than the beam size used in the 'large area'-measurements presented in the main manuscript. With increasing beam size, the degree of in-plane anisotropy within the beam-area decreases and the measurement

precision increases. Most importantly, the distribution average appears to be unaffected when changing the beam diameter.
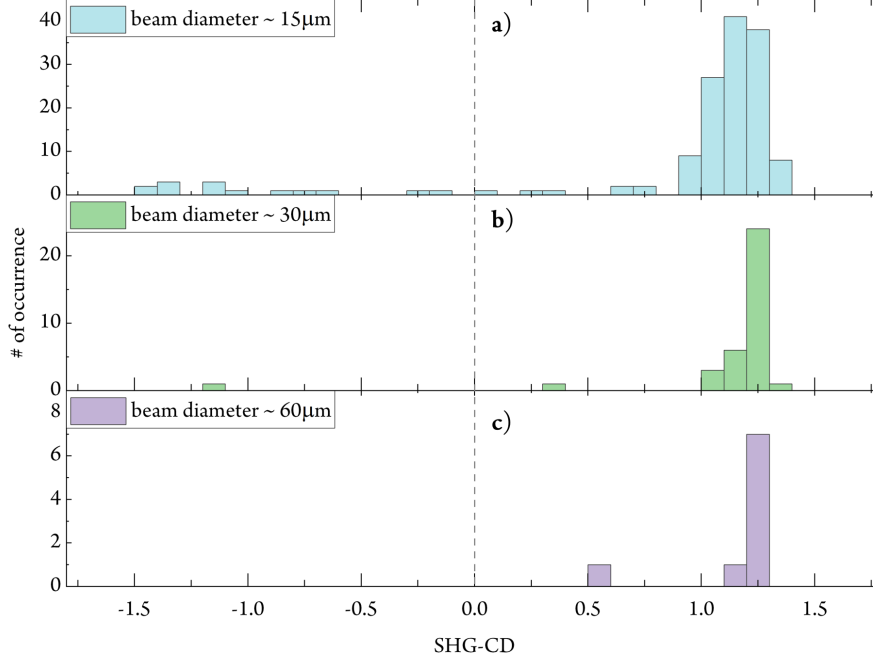

Figure S4: SHG-CD Histograms measured on enantiopure R-BINOL in front illumination configuration with different beam sizes (a) 15µm beam diameter. (b) 30µm, (c) 60µm.

Theoretical considerations

The nonlinear polarization and magnetization can be written as:

$$P_i^{(2)}(2\omega) = \varepsilon_0 \sum_{j,k} \left[\chi_{ijk}^{eee} E_j(\omega) E_k(\omega) + 2\chi_{ijk}^{eem} E_j(\omega) B_k(\omega) \right] \qquad \text{S3)}$$

$$M_i^{(2)}(2\omega) = \varepsilon_0 \sum_{j,k} \chi_{ijk}^{mee} E_j(\omega) E_k(\omega) \qquad \text{S4)}$$

As electric quadrupole and magnetic dipole components cannot be experimentally distinguished from each other, they are both usually contained in the non-local susceptibility elements χ_{ijk}^{eem} and χ_{ijk}^{mee}. Furthermore, the s- and p-components of the second harmonic generated electric field can be written as:

$$E_{s,p}(2\omega) = f_{s,p} E_p^2(\omega) + g_{s,p} E_s^2(\omega) + h_{s,p} E_s(\omega) E_p(\omega) \qquad \text{S5)}$$

5

where $f_{s,p}$, $g_{s,p}$ and $h_{s,p}$ are the field components for the transmitted second harmonic generation. In their most general form, these field components comprise of chiral and achiral nonlinear susceptibility tensor components and their origin can be electric or magnetic. For circularly polarized incident beam, $E_p(\omega) = \pm i E_s(\omega)$. Most importantly, by exercising Neumann's principle for cylindrical symmetry C_∞, the non-vanishing chiral susceptibility tensor components in the electric dipole approximation are: $\chi^{(2)}_{xyz} = \chi^{(2)}_{xzy} = -\chi^{(2)}_{yzx} = -\chi^{(2)}_{yxz}$, and the non-vanishing achiral components are: $\chi^{(2)}_{zzz}, \chi^{(2)}_{zxx} = \chi^{(2)}_{zyy}, \chi^{(2)}_{xxz} = \chi^{(2)}_{xzx} = \chi^{(2)}_{yyz} = \chi^{(2)}_{yzy}$. Note that the magnetic contributions and electric contributions beyond the second order for BINOL are negligible as shown by Hicks and Fischer.[5-6]

With Equation S5, the second harmonic intensity can be written as:

$$I_{s,p}(2\omega) = \left| -f_{s,p} + g_{s,p} \pm i h_{s,p} \right|^2 |E_s(\omega)|^4 \qquad \text{S6)}$$

Inserting Equation S6 into Equation 1 from the main manuscript, the numerator of the SHG-CD value can be written as Equation 2 from the main manuscript, or alternatively as:

$$SHG - CD_{s,p}(2\omega) \propto Im(h_{s,p}) \cdot Re(f_{s,p} - g_{s,p}) - Re(h_{s,p}) \cdot Im(f_{s,p} - g_{s,p}) \qquad \text{S7)}$$

Corresponding Authors

Aras Kartouzian - Catalysis Research Center and Chemistry Department, Chair of Physical Chemistry, Technische Universität München; Lichtenbergstr. 4, 85748 Garching, Germany; ORCID: 0000-0002-2193-2902; E-mail: aras.kartouzian@mytum.de

Hristo Iglev - Physik-Department E11, Technische Universität München; James-Franck-Str. 1, D-85748 Garching, Germany; ORCID: 0000-0001-9208-0068; E-mail: hristo.iglev@tum.de

References

1.   Ristow, F.; Scheffel, J.; Xu, X.; Fehn, N.; Oberhofer, K. E.; Riemensberger, J.; Mortaheb, F.; Kienberger, R.; Heiz, U.; Kartouzian, A., Understanding laser desorption with circularly polarized light. Chirality 2020, 32 (12), 1341-1353.

2.   von Weber, A.; Hooper, D. C.; Jakob, M.; Valev, V. K.; Kartouzian, A.; Heiz, U., Circular Dichroism and Isotropy–Polarity Reversal of Ellipticity in Molecular Films of 1, 1'-Bi-2-Naphtol. ChemPhysChem 2019, 20 (1), 62-69.

3.   Sauerbrey, G., Verwendung von Schwingquarzen zur Wägung dünner Schichten und zur Mikrowägung. Zeitschrift für physik 1959, 155 (2), 206-222.

4.   Kuroda, R.; Mason, S. F., The crystal and molecular structure of R-(–)-1, 1′-binaphthyl: the conformational isomerism and a comparison of the chiral with the racemic packing mode. Journal of the Chemical Society, Perkin Transactions 2 1981, (1), 167-170.

5.   Byers, J. D.; Hicks, J. M., Electronic spectral effects on chiral surface second harmonic generation. Chemical physics letters 1994, 231 (2-3), 216-224.

6.   Fischer, P.; Wise, F.; Albrecht, A., Chiral and achiral contributions to sum-frequency generation from optically active solutions of binaphthol. The Journal of Physical Chemistry A 2003, 107 (40), 8232-8238.